International Journal of Solids and Structures 49 (2012) 3063–3076

Contents lists available at SciVerse ScienceDirect

International Journal of Solids and Structures

journal homepage: www.elsevier.com/locate/ijsolstr

Multiaxial ratcheting with advanced kinematic and directional distortional hardening rules

Heidi P. Feigenbaum [a,*], Joel Dugdale [a], Yannis F. Dafalias [b,c], Kyriakos I. Kourousis [c], Jiri Plesek [d]

[a] Department of Mechanical Engineering, Northern Arizona University, Flagstaff, AZ 86011, USA
[b] Department of Civil and Environmental Engineering, University of California, Davis, CA 95616, USA
[c] Department of Mechanics, Faculty of Applied Mathematical and Physical Science, National Technical University of Athens, Zographou 15780, Greece
[d] Institute of Thermomechanics, Academy of Sciences of the Czech Republic, Prague, Czech Republic

ARTICLE INFO

Article history:
Received 21 December 2011
Received in revised form 31 May 2012
Available online 26 June 2012

Keywords:
Plasticity
Directional distortional hardening
Thermodynamics
Cyclic loading
Ratcheting

ABSTRACT

Ratcheting is defined as the accumulation of plastic strains during cyclic plastic loading. Modeling this behavior is extremely difficult because any small error in plastic strain during a single cycle will add to become a large error after many cycles. As is typical with metals, most constitutive models use the associative flow rule which states that the plastic strain increment is in the direction normal to the yield surface. When the associative flow rule is used, it is important to have the shape of the yield surface modeled accurately because small deviations in shape may result in large deviations in the normal to the yield surface and thus the plastic strain increment in multi-axial loading. During cyclic plastic loading these deviations will accumulate and may result in large errors to predicted strains.

This paper compares the bi-axial ratcheting simulations of two classes of plasticity models. The first class of models consists of the classical von Mises model with various kinematic hardening (KH) rules. The second class of models introduce directional distortional hardening (DDH) in addition to these various kinematic hardening rules. Directional distortion describes the formation of a region of high curvature on the yield surface approximately in the direction of loading and a region of flattened curvature approximately in the opposite direction. Results indicate that the addition of directional distortional hardening improves ratcheting predictions, particularly under biaxial stress controlled loading, over kinematic hardening alone.

1. Introduction

Ratcheting is the accumulation of plastic strains during cyclic plastic loading. Modeling this behavior is extremely difficult because any small systematic error in plastic strain during a single cycle will add to become a large error after many cycles. Most constitutive models for metals use the associative flow rule which states that the plastic strain increment is in the direction normal to the yield surface. When the associative flow rule is used, it is important to have the shape of the yield surface modeled accurately because small deviations in shape may result in large deviations in the normal to the yield surface and thus the plastic strain increment in multi-axial loading (this is not an issue in uniaxial loading because the normal to the yield surface remains the same with and without distortion). During cyclic plastic loading these deviations will accumulate and may result in large errors to predicted strains.

This paper compares the bi-axial ratcheting predictions of two classes of plasticity models. The first class of models consists of the classical von Mises model with various advanced kinematic hardening (KH) rules. The second class of models introduce directional distortional hardening (DDH) in addition to these various kinematic hardening rules. Directional distortion describes the formation of a region of high curvature on the yield surface approximately in the direction of loading and a region of flattened curvature approximately in the opposite direction. Such distortion has been observed in numerous experiments on various types of metals, including, but not limited to, those by Phillips et al. (1975), Naghdi et al. (1958), McComb (1960), Wu and Yeh (1991), and Boucher et al. (1995).

The kinematic hardening rules of interest will be described in Section 2 and the directional distortional hardening models of interest will be described in Section 3. Section 4 discusses the calibration of the models and Section 5 shows how the various models simulate bi-axial ratcheting tests. The results will include various KH rules with and without DDH as well as a few different forms of the DDH models. Simulations will be compared with

* Corresponding author. Tel.: +1 928 523 5326; fax: +1 928 523 2300.
E-mail addresses: heidi.feigenbaum@nau.edu (H.P. Feigenbaum), jwd42@nau.edu (J. Dugdale), jfdafalias@ucdavis.edu (Y.F. Dafalias), kourousi@central.ntua.gr (K.I. Kourousis), plesek@it.cas.cz (J. Plesek).

0020-7683/$ - see front matter © 2012 Elsevier Ltd. All rights reserved.
http://dx.doi.org/10.1016/j.ijsolstr.2012.06.006

experimental findings from Hassan and Kyriakides (1992), Hassan et al. (1992), and Corona et al. (1996).

In terms of notation, henceforth all second order tensors will be denoted by bold face in direct notation, e.g. $\boldsymbol{m}$, and all fourth order tensors will be capitalized in bold and calligraphy, e.g. $\boldsymbol{\mathcal{M}}$. No bold face symbols will be used when indexed components of tensors are used and a superposed do will indicate the rate. The proposed constitutive model is confined to small deformations. The stress tensor is denoted by $\boldsymbol{\sigma}$ and the linearized strain tensor is denoted by $\boldsymbol{\varepsilon}$. As usual, the strain tensor is decomposed into elastic and plastic parts ($\boldsymbol{\varepsilon} = \boldsymbol{\varepsilon}^e + \boldsymbol{\varepsilon}^p$) and the elastic constitutive law will be assumed linear and isotropic.

2. Kinematic hardening models

There are numerous kinematic hardening rules that were designed to help improve ratcheting predictions. This paper will focus on a few more recent kinematic hardening rules, and in particular those presented in Dafalias and Feigenbaum (2011), and the building blocks that lead to those models.

All kinematic hardening rules to be used in this work are based on the Armstrong and Frederick (1966) kinematic hardening rule, also known as the evanescence memory model, and referred to here as the AF model for abbreviation. The AF model is obtained by adding a dynamic recovery term to Prager's linear kinematic hardening term, Prager (1956)[1] which is directed along the current value of the back stress. Furthermore, all kinematic hardening rules to be used in this work have the back-stress additively decomposed into components, as first suggested by Chaboche et al. (1979). Initially it was suggested that each component obeys its own AF rule, thus this model can appropriately be named the multicomponent AF model (abbreviated MAF). In the present work, the back-stress will be additively decomposed into four components and the hardening rules for each component will not be purely the AF model, but rather more advanced models based on the AF formulation.

In particular, the kinematic hardening models to be used in this work will all make use of the modification to the MAF kinematic hardening rule suggested by Delobelle et al. (1995), which incorporates the Burlet and Cailletaud (1986) model, and therefore will be referred to as the BCD modification. Delobelle et al. suggested a non-linear kinematic hardening rule whose dynamic recovery term is a weighted average of regular AF type along the back stress, and a so-called radial evanescence rule along the plastic strain rate direction introduced by Burlet and Cailletaud (1986). In the original work, Delobelle et al. (1995) suggest either a fixed weighting factor or an empirically varied one. A very important property of this modification is that the value of the plastic modulus is unchanged from what it would be if the kinematic hardening was that of a simple AF kind for any type of loading, as was shown in the original papers and again more recently in Dafalias and Feigenbaum (2011). It follows that the main goal of this modification is to address the multiaxial ratcheting by modifying the change in the direction of the plastic strain increment via the ensuing change of the direction of kinematic hardening, while the uniaxial response remains unchanged from that of an AF model because of the invariance of the plastic modulus.

This BCD modification will be incorporated in the threshold model by Chaboche (1991) and multiplicative AF model by Dafalias et al. (2008a). Because the threshold is the key feature the Chaboche model will be abbreviated MAFT (the multicomponent AF model with a threshold, hence the T at the end). Similarly since the multiplier is the key feature, the Dafalias et al. model will be abbreviated MAFM (the multicomponent AF model with a multiplier, hence the M at the end). Simulations in the current work do not include the MAFT or MAFM models without the BCD modification because Dafalias and Feigenbaum (2011) showed that the following models that incorporate the BCD modification into the MAFT or MAFM models better simulate ratcheting results, and these models are the KH rules to be use in the present work:

- MAFTδ: The MAFT model with the BCD modification (the δ at the end is because it is a key parameter in this model). This model was first suggested by Bari and Hassan (2002). The kinematic hardening rules for this model are given in Eqs. (5)–(7).
- MAFMδ: The MAFM model with the BCD modification (the δ at the end is because it is a key parameter in this model). This model was first presented in Dafalias and Feigenbaum (2011). The kinematic hardening rules for this model are given in Eqs. (8)–(10).
- MAFTr: The MAFT model with the r modification to the BCD suggestion (hence the r at the end). This model was first presented in Dafalias and Feigenbaum (2011). The kinematic hardening rules for this model are given in Eqs. (13)–(15) and (7).
- MAFMr: The MAFM model with the r modification to the BCD suggestion (hence the r at the end).This model was first presented in Dafalias and Feigenbaum (2011). The kinematic hardening rules for this model are given in Eqs. (11)–(13).

Subsequent sections present some of the history and basic formulation of these models as well as the MAFT and MAFM models. In these sections, all models will use a unit normal formulation of the associative flow rule. Therefore the flow rule will be given by

$$\dot{\boldsymbol{\varepsilon}}^p = \langle\lambda\rangle \boldsymbol{n} \tag{1}$$

where λ is the loading index (or plastic multiplier) and $\boldsymbol{n}$ is the unit normal to the yield surface, i.e. $\boldsymbol{n} = (\partial f/\partial \boldsymbol{\sigma})/|\partial f/\partial \boldsymbol{\sigma}|$. Had a non-unit normal formulation been used, the flow rule would have been $\dot{\boldsymbol{\varepsilon}}^p = \langle\lambda\rangle(\partial f/\partial \boldsymbol{\sigma})$, the difference between these two accounted for by an adjustment of the value of the plastic modulus by a factor depending on the quantity $|\partial f/\partial \boldsymbol{\sigma}|$ (it is also important if the λ is defined in terms of $\boldsymbol{n}$ or $\partial f/\partial \boldsymbol{\sigma}$).

2.1. MAFT kinematic hardening rule

In this model, first proposed by Chaboche (1991), the back-stress is additively decomposed into many components, as usual, and each component of back-stress has its own AF kinematic hardening rule, except one component has its hardening rule altered such that the dynamic recovery term becomes inactive within a threshold in stress space in which case the rule becomes Prager's linear kinematic hardening. Outside this threshold this particular back-stress component evolves according to its own AF kinematic hardening rule like the other components. The threshold is defined by a term inside McCauley brackets, therefore, a continuous monitoring of whether or not the threshold has been crossed is required, a feature with some degree of inconvenience in numerical implementation of the model. The main goal of the threshold concept is to properly modify the value of the plastic modulus for better fitting uniaxial ratcheting, although it has also some minor effect on the direction of kinematic hardening since it alters one AF component to a Prager linear kinematic hardening within the range of the threshold. Since the key new feature of this model is the threshold, it can be called the threshold model. This model generally over-predicts ratcheting strains for biaxial loading (Bari and Hassan, 2002). A similar but not identical concept was presented by Ohno and Wang (1993), where again the intention was

[1] It was brought to the attention of the authors by a reviewer that linear kinematic hardening may have been propose earlier by Prager (1935), however, the authors were unable to translate this paper.

to deactivate or reduce the dynamic recovery term for certain stress range and loading directions.

2.2. MAFM kinematic hardening rule

As first presented by Dafalias et al. (2008a) MAFM is the so-called multi-component AF kinematic hardening rule with multiplier. The basic structure of this model is the same as the multicomponent back stress, however, one of the back stress ($\boldsymbol{\alpha}_4$) components instead of considering both coefficients of its AF rate equation of evolution constants, the coefficient of the dynamic recovery term will be variable, enhanced by expressions associated with the rate evolution equation of another dimensionless second order internal variable ($\boldsymbol{\alpha}_4^*$) also evolving according to an AF rule, but which is not a back-stress component itself. This variable coefficient of the dynamic recovery term allows the pace at which a back-stress component approaches its saturation level to vary depending on the direction of loading and the distance from saturation.

Specifically the evolution of these components in multiaxial stress space is given by the following equations Dafalias et al. (2008a,b):

$$\dot{\boldsymbol{\alpha}}_i = \langle\lambda\rangle\sqrt{\frac{2}{3}}c_i\left(\sqrt{\frac{2}{3}}a_i^s\boldsymbol{n} - \boldsymbol{\alpha}_i\right) \quad (i = 1,2,3) \tag{2}$$

$$\dot{\boldsymbol{\alpha}}_4 = \langle\lambda\rangle\sqrt{\frac{2}{3}}\left[c_4 + \sqrt{\frac{3}{2}}c_4^*\left(\sqrt{\frac{2}{3}}a_4^{*s} - \boldsymbol{\alpha}_4^* : \boldsymbol{n}\right)\right]\left(\sqrt{\frac{2}{3}}a_4^s\boldsymbol{n} - \boldsymbol{\alpha}_4\right) \tag{3}$$

$$\dot{\boldsymbol{\alpha}}_4^* = \langle\lambda\rangle c_4^*\sqrt{\frac{2}{3}}\left(\sqrt{\frac{2}{3}}a_4^{*s}\boldsymbol{n} - \boldsymbol{\alpha}_4^*\right) \tag{4}$$

where c_i, a_i^s, c_i^*, and a_i^{*s} are all model constants. The various square roots of 2/3 or 3/2 in the above equations play the role of guaranteeing that under uniaxial stress loading Eqs. (2)–(4) yield their uniaxial stress loading counterparts as explained in Dafalias et al. (2008a,b).

Observe that the first three components of the back stress according to Eq. (2) obey a typical AF kinematic hardening rule. The a_i^s represents the saturation (limit) value of the uniaxial loading counterpart a of $\boldsymbol{\alpha}_i$. The c_i is the coefficient of the dynamic recovery term of the AF rule along $\boldsymbol{\alpha}_i$, and it had been taken outside the parentheses in Eqs. (2). The evolution of the fourth back stress component $\boldsymbol{\alpha}_4$ is given by Eq. (3) in which observe that the dynamic recovery coefficient c_4 has been enhanced by expressions associated with the rate evolution equation of another dimensionless second order internal variable, the multiplier $\boldsymbol{\alpha}_4^*$, also evolving according to an AF rule as per Eq. (4). The multiplier $\boldsymbol{\alpha}_4^*$ is not a component of the back stress $\boldsymbol{\alpha}$, and its only role is to modify appropriately the coefficient c_4 of the component $\boldsymbol{\alpha}_4$. One can show that the terms which enhance the value of c_4, i.e. the terms which are inside the same parentheses as c_4 in Eq. (3), are obtained by taking the trace of the product with $\boldsymbol{n}$, of the difference of the current value of the multiplier $\boldsymbol{\alpha}_4^*$ from its saturation value $\sqrt{(2/3)}a_4^{*s}\boldsymbol{n}$ in multiaxial stress space, i.e., $\sqrt{\frac{2}{3}}a_4^{*s} - \boldsymbol{\alpha}_4^* : \boldsymbol{n} = \left(\sqrt{\frac{2}{3}}a_4^{*s}\boldsymbol{n} - \boldsymbol{\alpha}_4^*\right) : \boldsymbol{n}$. During a change in loading direction, this enhancement will generally speed up the evolution of $\boldsymbol{\alpha}_4$, since $\boldsymbol{\alpha}_4^* : \boldsymbol{n}$ will generally be smaller in value when $\boldsymbol{n}$ abruptly changes.

Again all these square roots terms of 2/3 and 3/2 lead to the exact uniaxial counterpart presented in Dafalias et al. (2008a,b) (one must also account for the relation $\boldsymbol{\alpha}_4^* : \boldsymbol{n} = \sqrt{(2/3)}\alpha_4^*$). Variability of the coefficients of an AF back-stress evolution law has been introduced in the past in various forms for improving ratcheting simulations, e.g. Chaboche (1991), Guionnet (1992), Ohno and Wang (1993), but not in a format involving their multiplication by another directionally evolving internal variable like the multiplier in the MAFM model.

Dafalias et al. (2008a) show that such multiplicative AF kinematic hardening rule combined with the underlying additive back-stress decomposition of the multicomponent hardening model can offer improvement in the simulation of the loops created by unloading/partial reverse loading/reloading, without sacrificing the ability to model the ratcheting response that is often improved because it is ultimately related to the underlying realistic modeling of such loops. They also show that the multiplicative AF scheme can substitute for the threshold refinement proposed by Chaboche (1991), i.e. the MAFT model, and elaborated by Bari and Hassan (2000) in uniaxial ratcheting simulations with equal and often slightly better success. Dafalias and Feigenbaum (2011) show that this model can also substitute for the MAFT model in bi-axial strain controlled ratcheting, again with approximately equal success.

2.3. MAFTδ and MAFMδ kinematic hardening rules

Bari and Hassan (2002) incorporated the BCD modification to a model where the back-stress is additively decomposed in AF components and one back-stress has a threshold as suggested by Chaboche (1991) (MAFT), in what can be symbolized by the acronym MAFTδ as explained previously. The result is the following kinematic hardening rule, adjusted as usual to reflect the unit normal formulation $\dot{\boldsymbol{\varepsilon}}^p = \langle\lambda\rangle\boldsymbol{n}$ and expressed in terms of the constants $c_i = \gamma_i$ and $a_i^s = C_i/\gamma_i$ instead of the originally used constants γ_i and C_i:

$$\dot{\boldsymbol{\alpha}}_i = \langle\lambda\rangle\sqrt{\frac{2}{3}}c_i\left\{\sqrt{\frac{2}{3}}a_i^s\boldsymbol{n} - [\delta\boldsymbol{\alpha}_i + (1-\delta)(\boldsymbol{\alpha}_i : \boldsymbol{n})\boldsymbol{n}]\right\} \quad (i = 1,2,3) \tag{5}$$

$$\dot{\boldsymbol{\alpha}}_4 = \langle\lambda\rangle\sqrt{\frac{2}{3}}c_i\left\{\sqrt{\frac{2}{3}}a_4^s\boldsymbol{n} - [\delta\boldsymbol{\alpha}_4 + (1-\delta)(\boldsymbol{\alpha}_4 : \boldsymbol{n})\boldsymbol{n}]\left\langle 1 - \frac{\bar{a}}{f(\boldsymbol{\alpha}_4)}\right\rangle\right\} \tag{6}$$

where $\bar{a}$ is the threshold level of back-stress that makes the dynamic recovery term inactive within the threshold, and $f(\boldsymbol{\alpha}_4)$ is defined as:

$$f(\boldsymbol{\alpha}_4) = \left[\frac{3}{2}\boldsymbol{\alpha}_4 : \boldsymbol{\alpha}_4\right]^{1/2} \tag{7}$$

Bari and Hassan assume δ (symbolized in their paper by δ') is a constant; in particular, they found best results for CS 1026 with $\delta = 0.18$.

Notice that each one of the equations given in Eqs. (5) and (6) use the BCD modification and Eq. (6) has the additional feature of the threshold term with the McCauley brackets $\langle\ \rangle$, multiplying the dynamic recovery component. One can observe that application of the consistency condition and use of Eqs. (5) and (6) renders the value of the hardening plastic modulus equal to a sum of terms each one of which is proportional to a quantity $c_i(\sqrt{2/3}a_i^s - \boldsymbol{\alpha}_i : \boldsymbol{n})$, $i = 1, 2, 3, 4$ (for the $\boldsymbol{\alpha}_4$ the threshold term multiplies $\boldsymbol{\alpha}_4 : \boldsymbol{n}$), hence, the modulus is independent of δ and identical to what it would have been obtained had the BCD modification not been introduced at all.

There is, however, a theoretical weakness of this model, and in fact this theoretical weakness extents to any models that use the Delobelle et al. (1995) or Burlet and Cailletaud (1986) kinematic hardening rules. As Dafalias and Feigenbaum (2011) rigorously show, the resulting kinematic hardening model might allow some or all of the back-stress components to move outside their natural saturation (limit) levels in stress space (a kind of bounding surface for back stress) depending on the value of the weighting factor δ, with consequences of a negative plastic modulus and an ensuing softening response while such response is not expected or sought. Dafalias and Feigenbaum show that restricting δ to the range

$0.5 \leqslant \delta \leqslant 1$ is necessary and sufficient to prohibit this unexpected and undesired possibility. Note that despite the unexpected and undesired possibility of softening, the BCD modification is thermodynamically admissible for all δ.

Since the choice of $\delta = 1$, gives the AF kinematic hardening rule, and since Bari and Hassan found that $\delta = 0.18$ gives the best results for many of the ratcheting experiments which will be modeled in this work, albeit with the aforementioned deficiency since $\delta < 0.5$, only the case of $\delta = 0.5$ will be used in the present study.

Proceeding in a similar manner as Bari and Hassan (2002) for the multicomponent model with a threshold, introduction of the BCD modification into the multicomponent AF with multiplier kinematic hardening model (MAFM), given in Eqs. (2)–(4), yields the following kinematic hardening rule symbolized by the acronym MAFMδ as explained in the previous section:

$$\dot{\boldsymbol{\alpha}}_i = \langle\lambda\rangle\sqrt{\frac{2}{3}}c_i\left[\sqrt{\frac{2}{3}}a_i^s\boldsymbol{n} - [\delta\boldsymbol{\alpha}_i + (1-\delta)(\boldsymbol{\alpha}_i:\boldsymbol{n})\boldsymbol{n}]\right] \quad (i=1,2,3) \tag{8}$$

$$\dot{\boldsymbol{\alpha}}_4 = \langle\lambda\rangle\sqrt{\frac{2}{3}}\left[c_4 + \sqrt{\frac{3}{2}}c_4^*\left(\sqrt{\frac{2}{3}}a_4^{*s} - \boldsymbol{\alpha}_4^*:\boldsymbol{n}\right)\right]\left(\sqrt{\frac{2}{3}}a_4^s\boldsymbol{n} - [\delta\boldsymbol{\alpha}_4 + (1-\delta)(\boldsymbol{\alpha}_4:\boldsymbol{n})\boldsymbol{n}]\right) \tag{9}$$

$$\dot{\boldsymbol{\alpha}}_4^* = \langle\lambda\rangle c_4^*\sqrt{\frac{2}{3}}\left(\sqrt{\frac{2}{3}}a_4^{*s}\boldsymbol{n} - \boldsymbol{\alpha}_4^*\right) \tag{10}$$

where again $\boldsymbol{\alpha} = \sum\boldsymbol{\alpha}_i$. Notice that the BCD modification was not introduced in the evolution law of the multiplier $\boldsymbol{\alpha}_4^*$ given by Eq. (10), but only in the evolution laws of the back-stress components $\boldsymbol{\alpha}_i$ in terms of a common weighting factor δ. The only difference between the present multiplicative AF model with the BCD modification (MAFMδ model) and that by Bari and Hassan (2002) (MAFTδ model) presented before, is the use of the multiplier rather than the threshold when comparing Eq. (9) and Eq. (6). Again, to avoid the potential for negative plastic modulus and softening (Dafalias and Feigenbaum, 2011), $\delta = 0.5$ will be chosen.

2.4. MAFTr and MAFMr kinematic hardening rules

As already mentioned the condition on δ required for not possibly crossing the bounding surface associated with the evolution of back stress given by is $0.5 \leqslant \delta \leqslant 1$. Focusing on the MAFM$\delta$ model (equivalent proposition can be made for the MAFTδ model), in order to remove the possibility of crossing the corresponding bounding surface by any one of the back-stress components, the following variation of the BCD modification was proposed by Dafalias and Feigenbaum (2011):

$$\dot{\boldsymbol{\alpha}}_i = \langle\lambda\rangle\sqrt{\frac{2}{3}}c_i\left[\sqrt{\frac{2}{3}}a_i^s\boldsymbol{n} - [r_i\boldsymbol{\alpha}_i + (1-r_i)(\boldsymbol{\alpha}_i:\boldsymbol{n})\boldsymbol{n}]\right] \quad (i=1,2,3) \tag{11}$$

$$\dot{\boldsymbol{\alpha}}_4 = \langle\lambda\rangle\sqrt{\frac{2}{3}}\left[c_4 + \sqrt{\frac{3}{2}}c_4^*\left(\sqrt{\frac{2}{3}}a_4^{*s} - \boldsymbol{\alpha}_4^*:\boldsymbol{n}\right)\right]\left(\sqrt{\frac{2}{3}}a_4^s\boldsymbol{n} - [r_4\boldsymbol{\alpha}_4 + (1-r_4)(\boldsymbol{\alpha}_4:\boldsymbol{n})\boldsymbol{n}]\right) \tag{12}$$

where r_i is given by:

$$r_i = \frac{\sqrt{(3/2)\boldsymbol{\alpha}_i:\boldsymbol{\alpha}_i}}{a_i^s} \tag{13}$$

This model is called the MAFMr model. Notice that Eqs. (11) and (12) are the same as Eqs. (8) and (9) but the variables r_i have replaced the constant δ. The same condition obtained for δ, i.e. $0.5 \leqslant r_i \leqslant 1$, guarantees that no crossing of the corresponding bounding surface for each $\boldsymbol{\alpha}_i$ can occur. According to its definition by Eq. (13), the value of r_i, which measures the proximity of $\boldsymbol{\alpha}_i$ to its saturation value $\boldsymbol{\alpha}_i^s = \sqrt{2/3}a_i^s\boldsymbol{n}$ on its bounding surface, will be between 0 and 1, and it will be equal to 1 at the crucial for crossing possibility point when $\boldsymbol{\alpha}_i = \boldsymbol{\alpha}_i^s$, therefore, the kinematic hardening becomes of the pure AF type and the possibility of the back-stress crossing its bounding surface and having a negative plastic modulus is eliminated. Because of the replacement of the BCD modification by a variation utilizing r_i (or r for a single back stress component), the variation will be called the r-modification. Identical variation where r_i substitute for δ can be applied to Eqs. (5)–(7) for the threshold model, in what can be called correspondingly the MAFTr model. Thus, the MAFTr model is defined as:

$$\dot{\boldsymbol{\alpha}}_i = \langle\lambda\rangle\sqrt{\frac{2}{3}}c_i\left\{\sqrt{\frac{2}{3}}a_i^s\boldsymbol{n} - [r_i\boldsymbol{\alpha}_i + (1-r_i)(\boldsymbol{\alpha}_i:\boldsymbol{n})\boldsymbol{n}]\right\} \quad (i=1,2,3) \tag{14}$$

$$\dot{\boldsymbol{\alpha}}_4 = \langle\lambda\rangle\sqrt{\frac{2}{3}}c_i\left\{\sqrt{\frac{2}{3}}a_4^s\boldsymbol{n} - [r_4\boldsymbol{\alpha}_4 + (1-r_4)(\boldsymbol{\alpha}_4:\boldsymbol{n})\boldsymbol{n}]\left\langle 1 - \frac{\bar{a}}{f(\boldsymbol{\alpha}_4)}\right\rangle\right\} \tag{15}$$

where again r_i is defined by Eq. (13) and $f(\boldsymbol{\alpha}_4)$ is defined by Eq. (7).

Notice that the r-modification eliminates the necessity to introduce the model constant δ.

3. Directional distortional hardening model (DDH)

Directional distortion has been modeled by Shutov et al. (2011), François (2001), Voyiadjis et al. (1990), and Kurtyka and Zyczkowski (1996), among others. The directional distortional models used in the present work are based on the work of Feigenbaum and Dafalias (2007, 2008) where all hardening rules are derived on the basis of sufficient conditions necessary to satisfy the dissipation inequality, in conjunction with a few simple, plausible assumptions about energy storage in the material. It should be noted that the thermodynamic derivation of these models is quite similar to that in Shutov et al. (2011).

For consistency with the original Feigenbaum and Dafalias (2007, 2008) work, a non-unit normal formulation of the associative flow rule will be used in this section. Therefore the flow rule will be given by

$$\dot{\boldsymbol{\varepsilon}}^p = \langle\lambda\rangle\frac{\partial f}{\partial\boldsymbol{\sigma}} \tag{16}$$

where λ is the loading index (or plastic multiplier). To switch to unit normal formulation, hardening rules and λ will need to be adjusted by a factor only depending on the quantity $|\partial f/\partial\boldsymbol{\sigma}|$.

The Feigenbaum and Dafalias (2007) model uses the following yield function:

$$f = (\boldsymbol{s}-\boldsymbol{\alpha}):[\mathcal{H}_0 + (\boldsymbol{n}_\mathbf{r}:\boldsymbol{\alpha})\mathcal{A}](\boldsymbol{s}-\boldsymbol{\alpha}) - k^2 = 0 \tag{17}$$

where $\boldsymbol{s}$ is the deviatoric component of the stress tensor, $\boldsymbol{\alpha}$ is the deviatoric back-stress tensor that represents the "center" of the yield surface, k represents the size of the yield surface, $\mathcal{A}$ is the fourth-order evolving anisotropic tensor, $\mathcal{H}_0$ is the fourth order isotropic unit tensor given by the expression $\mathcal{H}_{0_{ijkl}} = \frac{3}{2}\left[\frac{1}{2}\left(\delta_{ik}\delta_{jl} + \delta_{il}\delta_{jk}\right) - \frac{1}{3}\delta_{ij}\delta_{kl}\right]$, and $\boldsymbol{n}_\mathbf{r}$ is the radial, in regards to the center of the yield surface, deviatoric unit tensor illustrated in Fig. 1 and defined by

$$\boldsymbol{n}_\mathbf{r} = \frac{\boldsymbol{s}-\boldsymbol{\alpha}}{|\boldsymbol{s}-\boldsymbol{\alpha}|} \tag{18}$$

with the symbol $|\cdot|$ representing the norm of a tensor defined as $|\mathbf{m}| = \sqrt{\mathbf{m}:\mathbf{m}}$. The fourth order anisotropic tensor, $\mathcal{A}$, is responsible for distortional hardening in general, and the trace-type scalar multiplier, $\boldsymbol{n}_\mathbf{r}:\boldsymbol{\alpha}$, is responsible for the directionality of distortion. This can be intuitively understood if one observes that the double contraction $\boldsymbol{n}_\mathbf{r}:\boldsymbol{\alpha}$ is an inner product between the tensors $\boldsymbol{n}_\mathbf{r}$ and $\boldsymbol{\alpha}$, thus, it actually takes the "projection" of $\boldsymbol{\alpha}$ along the different "unit" directions $\boldsymbol{n}_\mathbf{r}$. This product can vary from $|\boldsymbol{\alpha}|$ to $-|\boldsymbol{\alpha}|$ passing through zero, and such variation effects the role of the distortional tensor $\mathcal{A}$ which is multiplied by it. Since the fourth-order tensor $\mathcal{A}$ is the corner stone of this model, it will henceforth be referred to as the "$\mathcal{A}$-model."

It must be mentioned that the introduction of an evolving fourth order tensor to describe non directional distortion and the

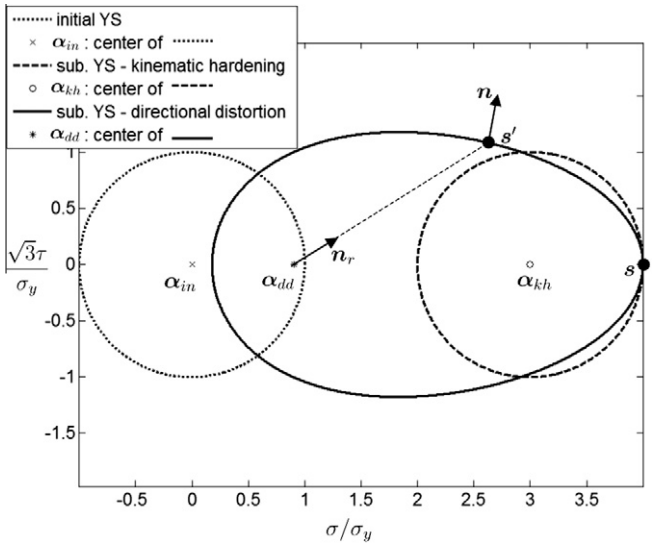

Fig. 1. Example of directional distortion of the yield surface for loading in pure tension. Observe the radial normal $\boldsymbol{n}_{\mathbf{r}}$ and how it differs from the unit normal $\boldsymbol{n}$. Also note that the two subsequent yield surfaces have the same final stress point in tension, but translation of the center of the directionally distorted yield surface is less than that with kinematic hardening alone.

thermodynamic basis of its evolution, was first presented in Dafalias et al. (2002).

Observe that due to the symmetry of $(s_{kl} - \alpha_{kl})$ in the indices k, l and the quadratic symmetry of Eq. (17), it follows without loss of generality that the following symmetry relations apply in reference to the components of $\mathcal{A}$

$$\mathcal{A}_{ijkl} = \mathcal{A}_{jikl} = \mathcal{A}_{klij} \tag{19}$$

Eqs. (19) reduce at first the number of independent components of $\mathcal{A}$ to 21, but because $(\boldsymbol{s} - \boldsymbol{\alpha})$ is deviatoric, it has five independent components with respect to an orthonormal basis, therefore, the independent components of $\mathcal{A}$ must reduce further from 21 to 15. This can be achieved by imposing the following six, single pair of indices traceless-type conditions, also referred to as incompressibility conditions, Dafalias (1979),

$$\mathcal{A}_{iikl} = 0 \tag{20}$$

where summation over repeated indices is implied.

In Feigenbaum and Dafalias (2008) two yield functions are proposed, the first of which can been understood as a special case of (17) where $\mathcal{A}$ is constantly aligned with the fourth order unit isotropic tensor $\mathcal{H}_0$ by means of a possibly varying proportionality factor, which gives rise to the following expression for the yield function:

$$f = \frac{3}{2}[1 - c(\boldsymbol{n}_{\mathbf{r}} : \boldsymbol{\alpha})](\boldsymbol{s} - \boldsymbol{\alpha}) : (\boldsymbol{s} - \boldsymbol{\alpha}) - k^2 = 0 \tag{21}$$

where c is a scalar-valued internal variable whose magnitude is directly associated with the amount of distortion of the yield surface. Since the back stress $\boldsymbol{\alpha}$ is the entity which dictates the directional distortion, this model will be referred to as the "$\boldsymbol{\alpha}$-model." For the purposes of this work, only this simplest version of the $\boldsymbol{\alpha}$-model will be considered, and this is the case where c is constant. Nonetheless the full $\boldsymbol{\alpha}$-model will be presented.

One criticism one might raise for the models in Eqs. (17) and (21) is that distortional hardening is coupled with kinematic hardening due to the role the back stress plays in the distortion scheme, while the underlying physics would imply an uncoupled consideration. To alleviate this problem a second yield function was proposed in Feigenbaum and Dafalias (2008),

$$f = \frac{3}{2}[1 - (\boldsymbol{n}_{\mathbf{r}} : \mathbf{r})](\boldsymbol{s} - \boldsymbol{\alpha}) : (\boldsymbol{s} - \boldsymbol{\alpha}) - k^2 = 0 \tag{22}$$

where $\mathbf{r}$ is a second order deviatoric tensor-valued directional distortional hardening internal variable. By introducing $\mathbf{r}$ in Eq. (22) the scalar quantity $\boldsymbol{n}_{\mathbf{r}} : \mathbf{r}$ is completely responsible for directional distortion, therefore, kinematic hardening has been decoupled from distortional hardening. Since $\mathbf{r}$ is the entity which dictates the directional distortion, this model will be referred to as the "$\mathbf{r}$-model." Notice the bold $\mathbf{r}$ represents the tensor responsible for distortion, which is not to be confused with the scalar r in the MAFTr and MAFMr which is a ratio that replaces the constant weighting factor in the BCD modification.

Thus the distortional hardening models to be use, can be summarized as follows:

- $\mathcal{A}$ model: This model was first suggested by Feigenbaum and Dafalias (2007). The key feature of this model is the fourth order tensor $\mathcal{A}$ which is responsible for distortion and the scalar multiplier $\boldsymbol{n}_{\mathbf{r}} : \boldsymbol{\alpha}$ which is responsible for the directionality of the distortion. The yield function for this model is given in Eq. (17). Note that in subsequent figures DDH refers to this model.
- $\boldsymbol{\alpha}$ model: This model was first suggested by Feigenbaum and Dafalias (2008). The key feature of this model is the scalar quantity $c(\boldsymbol{n}_{\mathbf{r}} : \boldsymbol{\alpha})$ which is responsible for distortion. It is called the $\boldsymbol{\alpha}$ model because the back-stress may be the only evolving quantity that leads to yield surface distortion. The yield function for this model is given in Eq. (21).
- $\mathbf{r}$ model: This model was first suggested by Feigenbaum and Dafalias (2008). The key feature of this model is the second order tensor $\mathbf{r}$ which is responsible for distortional hardening. The $\mathbf{r}$ allows kinematic hardening and distortional hardening to be decoupled. The yield function for this model is given in Eq. (22).

The hardening rules for these models are obtained from conditions sufficient for satisfaction of the second law of thermodynamics, in conjunction with a few simple and plausible assumptions about energy storage and release in the material. Details of these thermodynamic assumptions and how the hardening rules are sufficient to satisfy the second law of thermodynamics can be found in Feigenbaum and Dafalias (2007, 2008). For now only the hardening rules themselves along with some thermodynamically necessary restrictions will be presented.

All three models give rise to the same form of isotropic and kinematic hardening, however, isotropic hardening will not be included in any of the simulations in this work, and the kinematic hardening rules to be used have been described in a previous section.

The hardening rules that arise for the distortional parameters for the three models are as follows:

$$\dot{\mathcal{A}} = -\lambda A_1 |\boldsymbol{s} - \boldsymbol{\alpha}|^2 \left[(\boldsymbol{n}_{\mathbf{r}} : \boldsymbol{\alpha}) \boldsymbol{n}_{\mathbf{r}} \otimes \boldsymbol{n}_{\mathbf{r}} + \frac{3}{2} A_2 \mathcal{A} \right] \tag{23}$$

$$\dot{c} = \frac{3}{2} \lambda c_1 |\boldsymbol{s} - \boldsymbol{\alpha}|^2 [(\boldsymbol{n}_{\mathbf{r}} : \boldsymbol{\alpha}) - c_2 c] \tag{24}$$

$$\dot{\mathbf{r}} = \frac{3}{2} \lambda \rho_1 |\boldsymbol{s} - \boldsymbol{\alpha}|^2 (\boldsymbol{n}_{\mathbf{r}} - \rho_2 \mathbf{r}) \tag{25}$$

where A_1, A_2, c_1, c_2, ρ_1 and ρ_2 are non-negative material constants. These hardening rules are sufficient for the satisfaction of the second law of thermodynamics provided that

$$A_2 |\mathcal{A}|^2 \leqslant 1, \quad c_2 c^2 \leqslant 1, \quad \rho_2 |\mathbf{r}|^2 \leqslant 1 \tag{26}$$

for all time, where $|\mathcal{A}|^2 = \mathcal{A} :: \mathcal{A} = \mathcal{A}_{ijkl} \mathcal{A}_{ijkl}$, since $\mathcal{A}$ is symmetric, and $|\mathbf{r}|^2 = \mathbf{r} : \mathbf{r}$ are Euclidean norms (Feigenbaum and Dafalias, 2007, 2008).

Table 1
Material constants for CS 1026 with kinematic hardening only.

	MAFTδ	MAFMδ	MAFTr	MAFMr
c_1	20,000	20,000	20,000	20,000
a_1^s	3 ksi	3 ksi	3 ksi	3 ksi
c_2	400	400	400	400
a_2^s	8.07 ksi	8.07 ksi	8.07 ksi	8.07 ksi
c_3	11	10	11	10
a_3^s	41.4 ksi	45.5 ksi	41.4 ksi	45.5 ksi
c_4	5000	1800	5000	1800
a_4^s	3 ksi	8 ksi	3 ksi	8 ksi
$\bar{a}$	5 ksi	–	5 ksi	–
c_4^*	–	5000	–	5000
a_4^{s*}	–	0.16	–	0.16
δ	0.5	0.5	–	–

Table 2
Material constants for CS 1018 with kinematic hardening only.

	MAFTδ	MAFMδ	MAFTr	MAFMr
c_1	20,000	20,000	20,000	20,000
a_1^s	3 ksi	3 ksi	3 ksi	3 ksi
c_2	400	400	400	400
a_2^s	8.07 ksi	8.07 ksi	8.07 ksi	8.07 ksi
c_3	20	20	20	20
a_3^s	40 ksi	40 ksi	40 ksi	40 ksi
c_4	5000	600	5000	600
a_4^s	3 ksi	8 ksi	3 ksi	8 ksi
$\bar{a}$	5 ksi	–	5 ksi	–
c_4^*	–	5000	–	5000
a_4^{s*}	–	0.16	–	0.16
δ	0.5	0.5	–	–

Table 3
Distortional material parameters.

A_1	2.25 ksi^{-4}
A_2	1575 ksi^2
ρ_1	5 ksi^{-2}
ρ_2	6
c	0.0055 ksi^{-1}

Notice that all hardening rules for all models, and in particular for the evolution of the fourth order tensor $\mathcal{A}$, are of the evanescent memory type, therefore the internal variables all reach finite limits under any type of loading. These limits can be found by setting the rate equations in (23)–(25) equal to zero, which yields:

$$\mathcal{A}^l = -\frac{2\alpha^{\max}}{3A_2}\boldsymbol{n}_{\mathbf{r}}^l \otimes \boldsymbol{n}_{\mathbf{r}}^l \tag{27}$$

$$c^l = \frac{\alpha^{\max}}{c_2} \tag{28}$$

$$\mathbf{r}^l = \frac{1}{\rho_2}\boldsymbol{n}_{\mathbf{r}}^l \tag{29}$$

where the superscript l denotes the limit values of the quantities involved. The quantity $\alpha^{\max}$, which appears in the equations of the limits for the distortional parameters for the $\mathcal{A}$ and $\boldsymbol{\alpha}$ models, Eqs. (27) and (28), is the magnitude of the limit back-stress. Specifically, $\alpha^{\max}$ is defined by

$$\boldsymbol{\alpha}^l = \alpha^{\max}\boldsymbol{n}^l = \alpha^{\max}\boldsymbol{n}_{\mathbf{r}}^l \tag{30}$$

for AF type kinematic hardening rules. The fact that $\boldsymbol{n}_{\mathbf{r}}^l = \boldsymbol{n}^l$ at the limit, as shown in Feigenbaum and Dafalias (2007, 2008), has been evoked to derived Eqs. (27)–(30). The magnitude of the limit back-stress, $\alpha^{\max}$ depends on the kinematic hardening rule used. For the MAFMδ and MAFMr the magnitude of the limit of the back-stress is:

$$\alpha^{\max} = |\boldsymbol{\alpha}^l| = \left|\sum_{i=1}^{4}\boldsymbol{\alpha}_i^l\right| = \sum_{i=1}^{4}\sqrt{\frac{2}{3}}a_i^s \tag{31}$$

Similarly, for the MAFTδ and MAFTr the magnitude of the limit of the back-stress is:

$$\alpha^{\max} = |\boldsymbol{\alpha}^l| = \left|\sum_{i=1}^{4}\boldsymbol{\alpha}_i^l\right| = \sum_{i=1}^{3}\sqrt{\frac{2}{3}}a_i^s + \sqrt{\frac{2}{3}}(a_4^s + \bar{a}) \tag{32}$$

Assuming that the maximum of the inequalities in (26) occurs at the limit, under any type of loading, the thermodynamic requirements in (26) give the following restrictions on material constants for the $\mathcal{A}$-model, $\boldsymbol{\alpha}$-model and $\mathbf{r}$-model, correspondingly:

$$\frac{A_2}{(\alpha^{\max})^2} \geqslant \frac{4}{9}, \quad \frac{c_2}{(\alpha^{\max})^2} \geqslant 1, \quad \rho_2 \geqslant 1 \tag{33}$$

Convexity of these models were proven in Plesek et al. (2010). For the $\boldsymbol{\alpha}$-model, $\mathbf{r}$-model, and $\mathcal{A}$-model convexity requires the following, respectively:

$$|c\boldsymbol{\alpha}| < 1, \quad |\mathbf{r}| < 1, \quad |\boldsymbol{\alpha}||\mathcal{A}|_\lambda < \frac{3}{2} \tag{34}$$

where $|\mathcal{A}|_\lambda$ is the maximum eigenvalue of $-\mathcal{A}$. Note that the inequalities for convexity in (34) represent necessary and sufficient conditions for the $\boldsymbol{\alpha}$ and $\mathbf{r}$ models, but only a necessary condition for the $\mathcal{A}$ model. A necessary and sufficient condition for the $\mathcal{A}$ model can only be found at the limit, assuming that is the most distorted yield surface. And in fact looking at the limit for all models gives restrictions on the parameters as follows:

$$\frac{c_2}{(\alpha^{\max})^2} > 1, \quad \rho_2 > 1, \quad \frac{A_2}{(\alpha^{\max})^2} > 0.55 \tag{35}$$

Notice that the convexity requirement is either the same or more stringent than the thermodynamic requirement, therefore if convexity is satisfied the thermodynamic requirement is automatically satisfied. For the $\boldsymbol{\alpha}$-model, if only constant c is considered, convexity is always guaranteed. The convexity requirements in (35) along with definitions of $\alpha^{\max}$ from Eqs. (31) and (32) will play an important role in the calibration of model parameters.

4. Calibration of models

The various kinematic hardening and directional distortional hardening rules will be used to fit experimental data on CS 1018 and CS 1026 from Hassan and Kyriakides (1992), Hassan et al. (1992) and Corona et al. (1996). The model parameters for CS 1026 with kinematic hardening alone are from Dafalias et al. (2008a) and Bari and Hassan (2000). For the convenience of the reader and easy comparison with subsequent models, these constants are presented in Table 1.

The model parameters for CS 1018 are slightly different than for CS 1026. However, the relevant parameters for CS 1026 have been used as a basis for the determination of the CS 1018 parameters, due to the fact that the two materials exhibit a very similar response. In particular, the calibration procedure involved the fine tuning of the CS 1026 parameters in terms of best fitting the stabilized CS 1018 stress–strain hysteresis loop, which was taken from published experimental results Corona et al. (1996). Table 2 shows the model parameters for CS 1018.

For the addition of distortion, the model parameters were determined by systematically and iteratively guessing and checking. While such a calibration technique is not ideal, it serves the

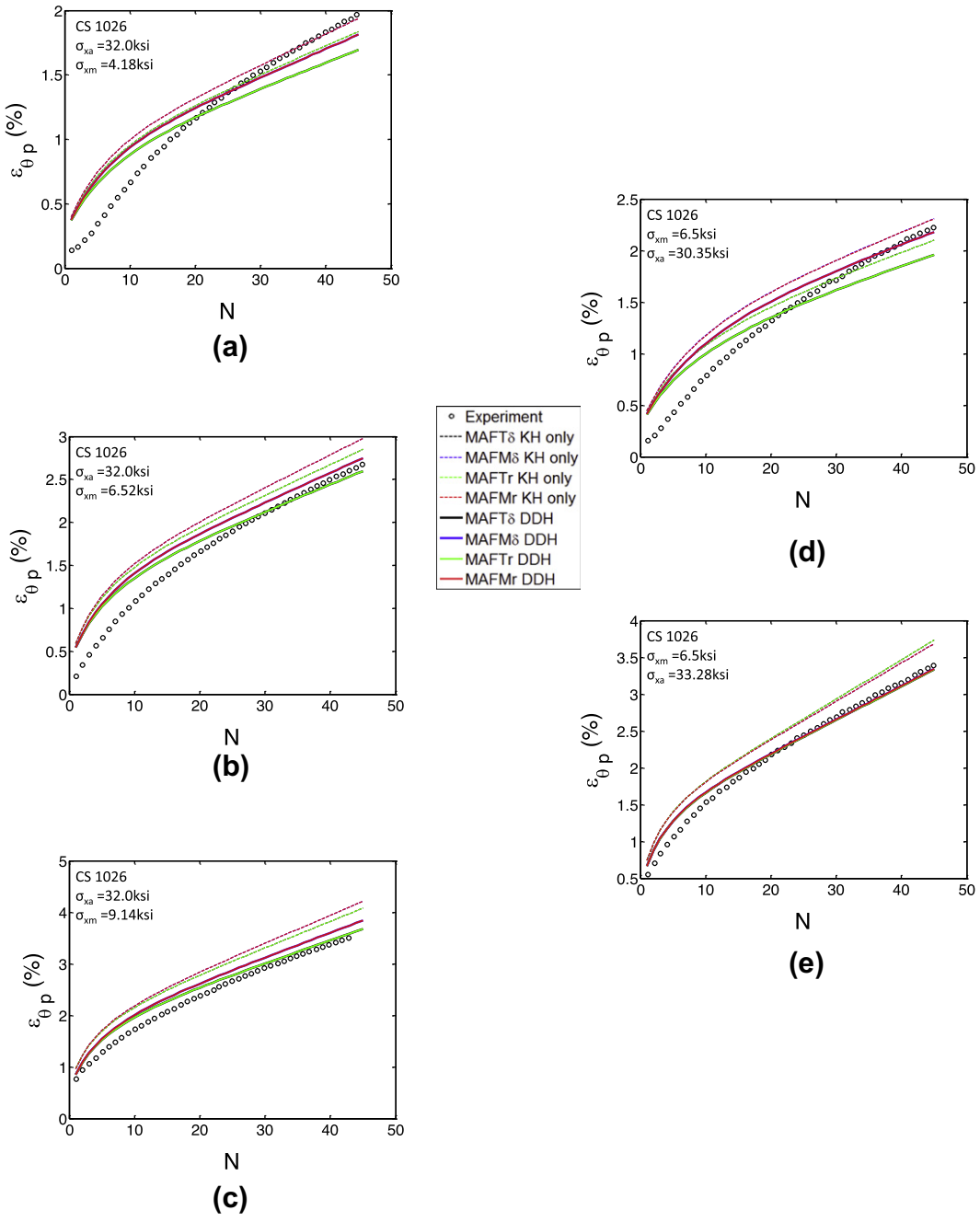

Fig. 2. Uniaxial ratcheting data from Hassan and Kyriakides (1992) with simulated various kinematic hardening rules with and without directional distortional hardening. In this case, DDH implies that the $\mathcal{A}$-model was used. Note that this data was used to calibrate the DDH model.

purposes of this work and allows one to determine which KH rule generally fits the ratcheting data best and how the addition of DDH improves the predictions of ratcheting. Current work is underway to develop a more rigorous means of calibrating the Feigenbaum and Dafalias (2007, 2008) DDH models.

As Fig. 1 shows, to reach the same stress point, less translation of the yield surface is needed when directional distortion is included. Therefore, the parameters must be changed so that the amount of kinematic hardening is decreased when directional distortional hardening is included. Specifically, values for c_1–c_3 and a_1^s–a_3^s were decreased in order to lessen the amount of kinematic hardening and allow room for distortional hardening to occur. Decreasing c_1–c_3 slowed the rate of kinematic hardening, while decreasing a_1^s–a_3^s lowered the limit of kinematic hardening. For simplicity, since the fourth kinematic hardening rule is unique in kind, the parameters associated with this fourth kinematic hardening rule were unchanged. Similarly, $\bar{a}$ in the threshold models was left unchanged.

Furthermore, for simplicity, it was assumed that change in the kinematic hardening parameters would be uniform, i.e. all kinematic hardening parameters would all change by an equal percentage. This was assumed because the different back-stresses are each associated with different regions of the stress–strain curve, however, there is no evidence to suggest that distortion of the yield surface primarily occurs in one region of the stress–strain curve. Moreover, if percentage change of the kinematic hardening parameters is the same across all models, since it is the same material, the same "amount" of directional distortion should occur.

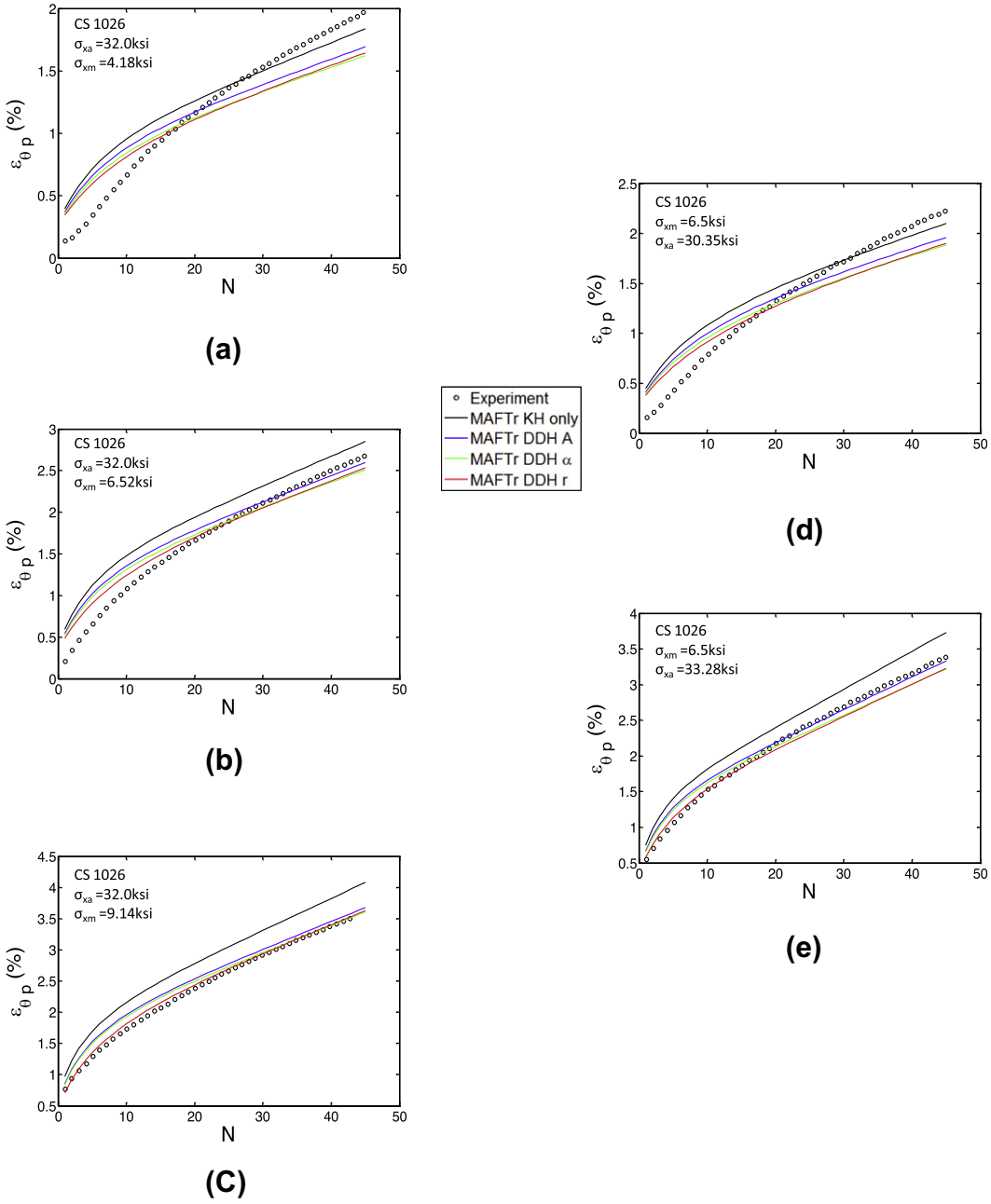

Fig. 3. Uniaxial ratcheting data from Hassan and Kyriakides (1992) simulated with the MAFTr kinematic hardening rule and the various directional distortional hardening models. Note that this data was used to calibrate the DDH models.

Once the kinematic hardening parameters were reduced, the distortional parameters were added with the convexity requirement in (35), where $\alpha^{\max}$ is given by Eq. (31) for the MAFM models or (32) for the MAFT models, used as a guide. The distortional parameters to be used were assumed to be the same vales no matter the kinematic hardening rule used. Again, this was because the same amount of distortion is expected for the same material.

The calibration was checked against strain symmetrically stabilized experimental data and uniaxial ratcheting experimental data from Hassan et al. (1992) and Hassan and Kyriakides (1992), respectively, on thin walled tubes of CS 1026. The strain symmetric stabilization was performed before the biaxial ratcheting tests, and it was found that the hysteresis loops stabilized fairly quickly. For the simulations, it was assumed that during the strain symmetric stabilization, the isotropic hardening would saturate and therefore isotropic hardening was not included in the modeling. The uniaxial ratcheting experiments were axially stress controlled loading of the thin walled tubes of CS 1026 at various mean stresses, σ_{xm}, and stress amplitudes, σ_{xa}. Iterations were performed until good fits were achieved for both sets of experimental data.

Ultimately the c_1—c_3 and a_1^s—a_3^s constants were only decreased by 1% from their original values for kinematic hardening alone, and the distortional parameters are given in Table 3. Simulation of uniaxial ratcheting, which was used for calibration, is shown in Figs. 2 and 3. Fig. 2 shows results using the different kinematic hardening rules with and without distortion. In this figure, with distortion implies the $\mathcal{A}$-model. Fig. 3 shows results for only one kinematic hardening rule, MAFTr, but with the different distortional models. In general, these figures show that all the models can accurately reproduce the uniaxial data to which they were calibrated. As

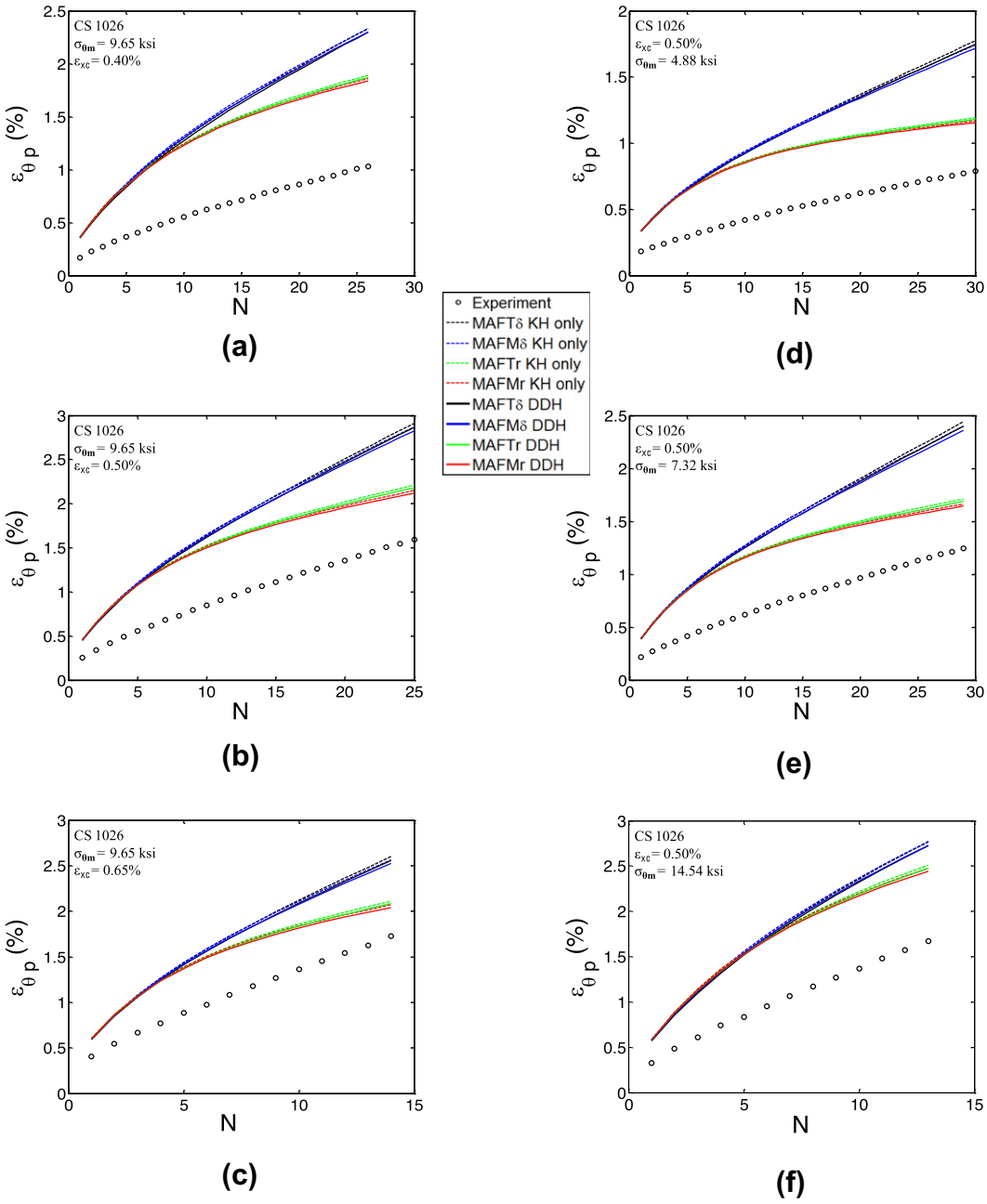

Fig. 4. Strain controlled biaxial ratcheting data simulated with various kinematic hardening rule with and without directional distortional hardening. In this case, with distortion implies that the $\mathcal{A}$-model was used.

expected, there is no advantage of using the distortional models to simulate the uniaxial ratcheting data since under uniaxial loading the normal to the yield surface will not change, with or without distortion, and thus neither will the direction of plastic strain. The simulation of the strain symmetrically stabilized curves are not reproduced here because they very closely match experimental data in all cases.

In order to add DDH with CS 1018, just as was done for CS 1026, the material parameters $c_1 - c_3$ and $a_1^s - a_3^s$ constants were decreased by 1% from their original values, given in Table 2, for kinematic hardening alone. Since the stabilized plot for CS 1018 is very similar to that for CS 1026, and since no uniaxial ratcheting data was available for CS 1018, the distortional parameters, A_1 and A_2, were assumed to be the same for the two materials and are given in Table 3. These parameters gave a good fit of the strain symmetrically stabilized curves found experimentally. The r and $\boldsymbol{\alpha}$ models for DDH were not used to simulate any CS 1018 data, therefore ρ_1, ρ_2, and c parameters were not calibrated for CS 1018.

5. Fitting of ratcheting data

5.1. Results

Figs. 4–6 show how the various kinematic hardening rules, with and without directional distortional hardening, simulate experimental results. For these figures, DDH refers to the $\mathcal{A}$-model. Figs. 7,8 show how different directional distortional hardening models simulate experimental ratcheting results.

The experimental data for Figs. 4,5 and Figs. 7,8 is from Hassan et al. (1992). In the experiments, thin walled tubes of carbon steel

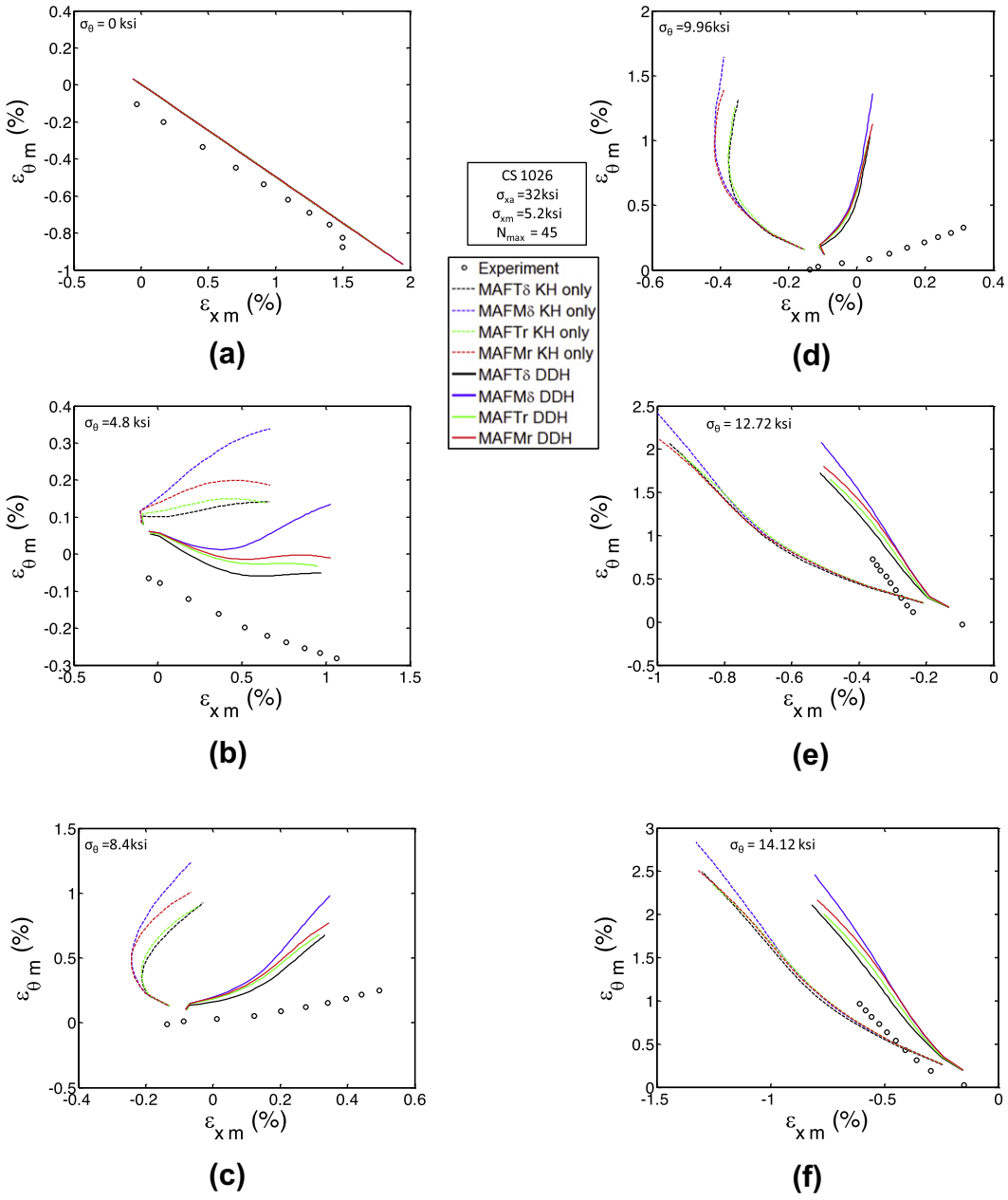

Fig. 5. Stress controlled biaxial ratcheting data simulated with various kinematic hardening rule with and without directional distortional hardening. In this case, with distortion implies that the $\mathcal{A}$-model was used.

1026 were first stabilized by strain symmetric axial cycles in the range of $\pm 1\%$ and in approximately 12 cycles the hysteresis loops were stable. Following the strain symmetric cycling the specimens were unloaded to approximately zero axial stress and strain, although typically some small residual circumferential strain remained non-zero. Note that when simulating the strain controlled biaxial ratcheting data in Figs. 4 and 7, the material was assumed to begin in a virgin state, i.e. the stabilization of the material was not simulated. However, when simulating the complex load paths and the stress controlled biaxial ratcheting in Figs. 5, 6 and 8, the stabilization was simulated before the ratcheting. Generally, simulating the stabilization makes little difference to the ratcheting predictions.

For the strain controlled results in Figs. 4 and 7, after the stabilization, Hassan et al. (1992) preloaded the tubes using stress control with various internal pressures. These internal pressures resulted in circumferential stress that vary between $\sigma_\theta = 0.120\sigma_0$ and $\sigma_\theta = 0.357\sigma_0$, where $\sigma_0 = 39.8$ ksi. The tubes were then cyclically loaded using strain control in the axial direction with various amplitude of the strain cycle ranging between $\boldsymbol{\varepsilon}_{xc} = 0.4\%$ and $\boldsymbol{\varepsilon}_{xc} = 0.65\%$, while the internal pressure remained constant.

For the stress controlled results in Figs. 5 and 8, after the stabilization, Hassan et al. (1992) preloaded the tubes using stress control with various internal pressures. While the internal pressure remained constant, the tubes were then cyclically loaded using stress control in the axial direction with various amplitudes of stress and various mean stress values. Figs. 5 and 8 show the mean axial strain ε_{xm} and the mean circumferential strain $\varepsilon_{\theta m}$ per cycle, which are both predicted values.

Fig. 6 shows how the various models perform in more complex paths. In this figure the experimental data is from Corona et al. (1996). The various load paths are shown in the figure, and include

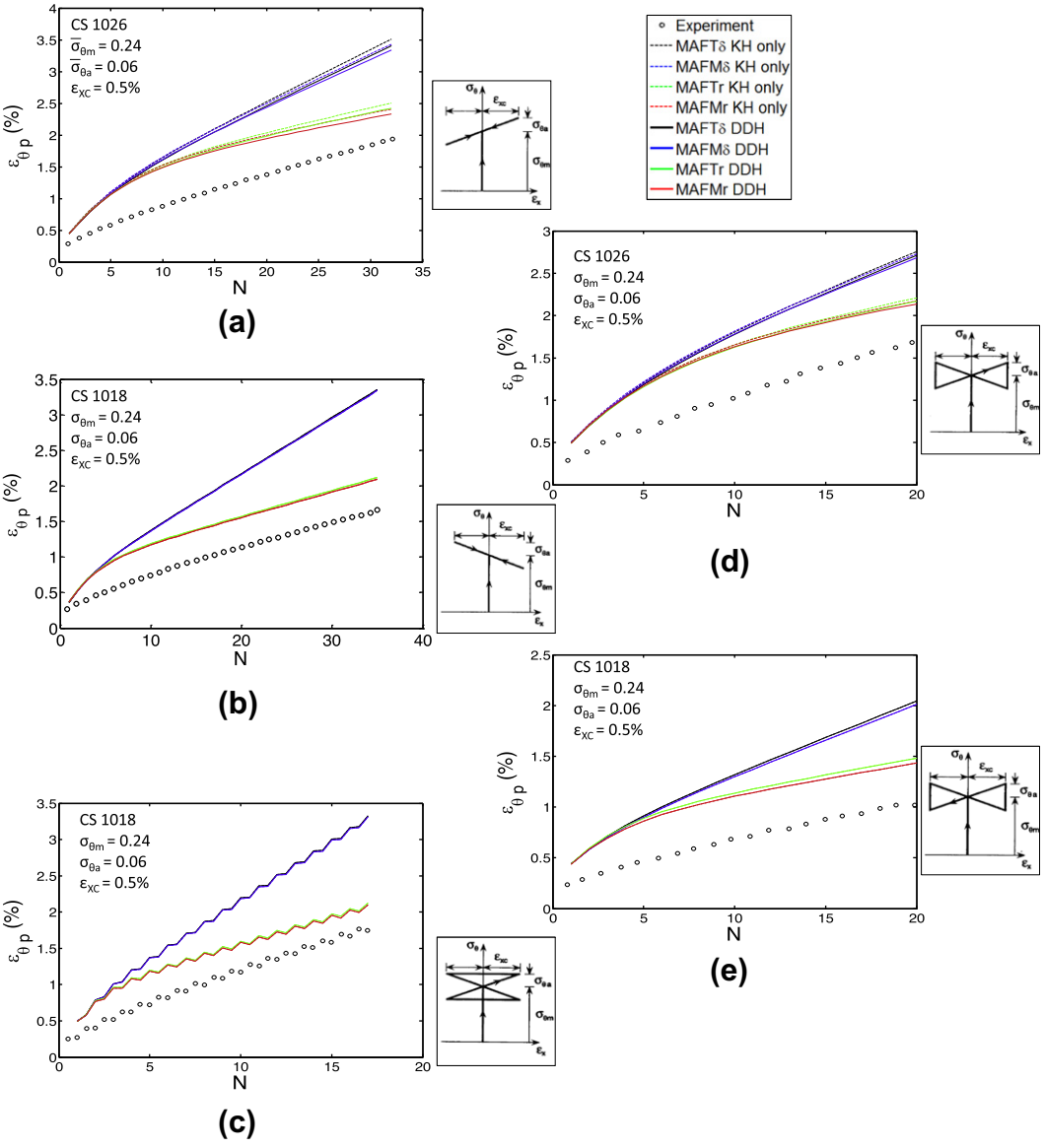

Fig. 6. Strain controlled biaxial ratcheting data from complex load paths simulated with various kinematic hardening rule with and without directional distortional hardening. In this case, with distortion implies that the $\mathcal{A}$-model was used.

a bowtie path, a reverse bowtie path, and hourglass path and two slanted paths. All these complex load paths are achieved using strain controlled loading. As with the Hassan et al. (1992) experimental results, the material was cyclically loaded symmetrically and stabilized before any ratcheting tests. Please note that in this figure, the experimental result in (b), (c) and (e) are from thin walled tubes of CS 1018. Observe that there is almost no difference between the simulated results with and without DDH for CS 1018, and only minimal difference for CS 1026.

5.2. Discussion

Comparing the different kinematic hardening models in Figs. 4 and 6 it can be seen that with strain controlled loading, which includes the complex load paths in Fig. 6, the MAFTr and MAFMr more accurately simulate the experimental data that the MAFTδ and MAFMδ models with $\delta = 0.5$. This fact might have been expected since Bari and Hassan (2002) choose to use a much smaller value of δ, 0.18, to simulate the same data. When $\delta = 0.5$ was chosen, to avoid the potential for softening, the model behaves more like the AF model and less like the Burlet and Cailletaud model, and thus ratcheting is over predicted, as is usually seen with the AF model.

These results suggest that when the BCD modification is used, the variable r given by Eq. (13) is preferred over the fixed δ. From the strain controlled biaxial ratcheting simulations in Figs. 4 and 6 it seems that the MAFMr kinematic hardening model most accurately matches experimental tests. However, Fig. 5 shows that MAFTr model performs constantly better than the MAFMr model in stress controlled loading. Therefore one might conclude that the MAFTr model overall performs the best out of the kinematic hardening rules used in this study without the use of DDH. This is why only the MAFTr model was used to compare the performance of the different directional distortional hardening models in Figs. 7 and 8.

However, given that the difference of the MAFTr from the MAFMr model simulations is not that great, while the latter has the advantage of avoiding the necessity to check if the threshold is exceeded at each step, the use of MAFMr can be often preferable than the use of MAFTr.

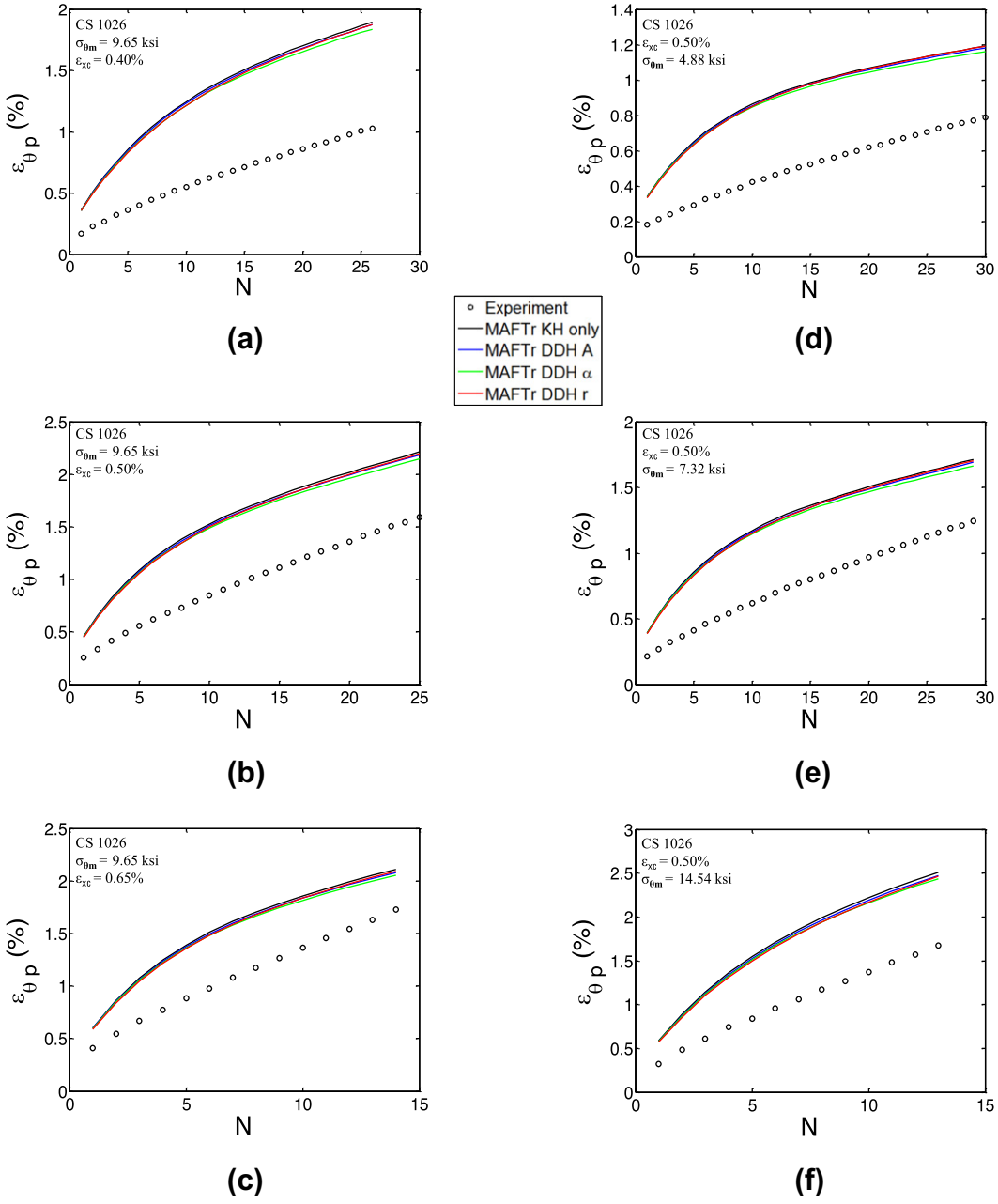

Fig. 7. Strain controlled biaxial ratcheting data simulated with the MAFTr kinematic hardening rule and various directional distortional models.

From Figs. 4 and 6 it can be seen that directional distortional hardening can improve predictions of strain controlled biaxial ratcheting, although only very minimally. Similar results in Fig. 7 show that virtually identical results are obtained for strain controlled biaxial ratcheting simulations with the various directional distortional models. This can be understood by the fact that minimal distortion occurs to the yield surface with the material parameters identified. For example, for the loading in Fig. 4a, using the MAFTr kinematic hardening rule, there is less than a 3% difference between all components of $\boldsymbol{n}_r$ versus the same components of $\boldsymbol{n}$. Other load conditions give similar very small differences between $\boldsymbol{n}_r$ and $\boldsymbol{n}$. Since directional distortional hardening makes little difference in results for the complex load paths in Fig. 6, these load conditions were not simulated with the various different directional distortional models.

For stress controlled ratcheting the results are much different. Fig. 5 shows that consistently the inclusion of directional distortional hardening improves stress controlled biaxial ratcheting predictions, often significantly. The only exception to this significant improvement of predictions is Fig. 5a, where there is zero internal pressure, so it is merely uniaxial ratcheting where it is not expected for distortion to make an improvement.

Fig. 8 suggests that, while inclusion of directional distortion very much improves stress controlled biaxial ratcheting predictions, the choice of the directional distortional model makes little difference. Therefore, one may choose to work with the $\boldsymbol{\alpha}$-model since it is the simplest and gives approximately as accurate results as the more complicated directional distortional models.

6. Conclusion

In this work, it was shown that directional distortional hardening improves ratcheting predictions, particularly biaxial

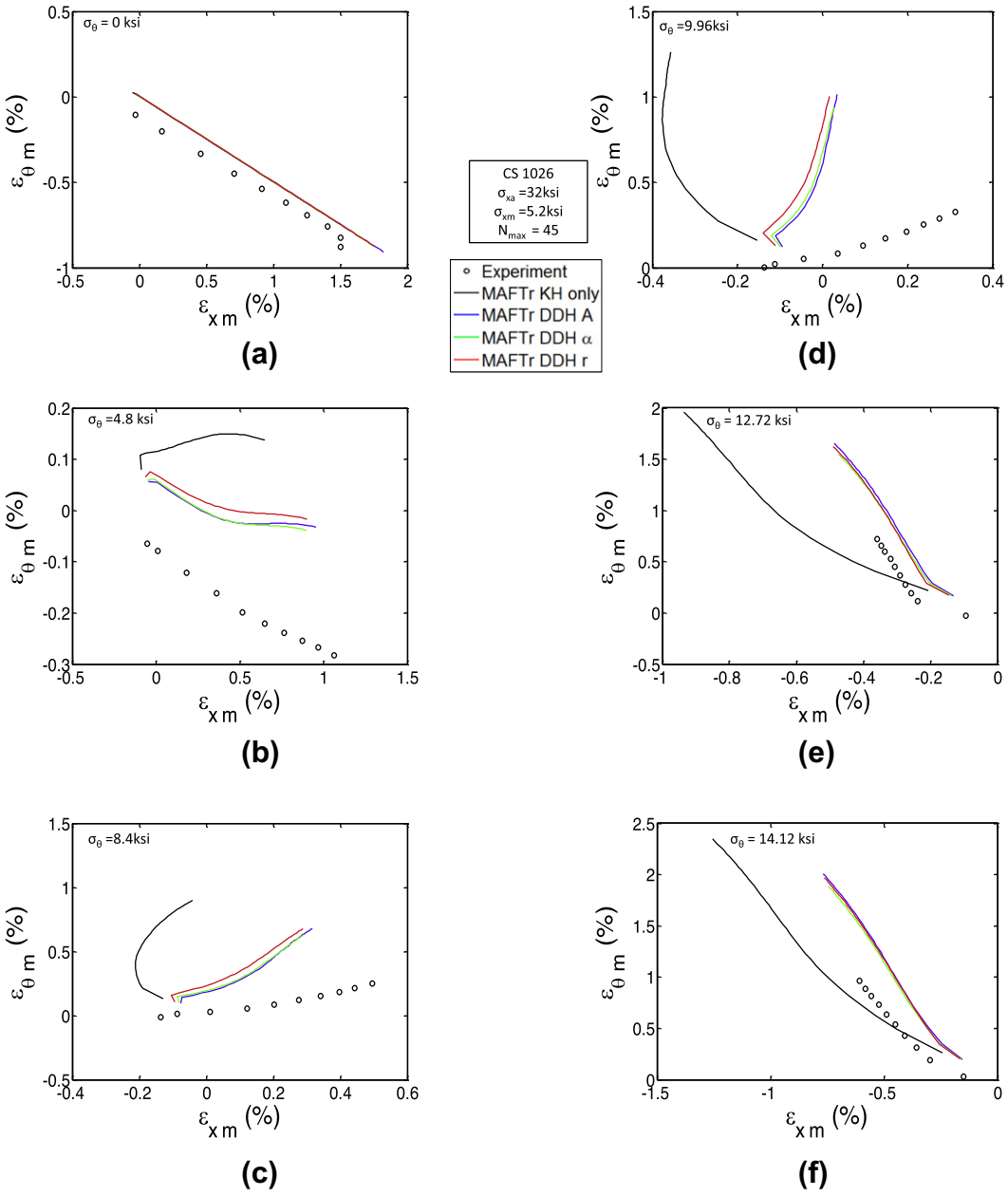

Fig. 8. Stress controlled biaxial ratcheting data simulated with the MAFTr kinematic hardening rule and various directional distortional models.

stress controlled predictions, over kinematic hardening alone. Furthermore, it was shown that of the different directional distortional hardening models used, there seemed to be fairly little difference in the accuracy of ratcheting simulations, therefore one may choose to use the simplest model, the $\boldsymbol{\alpha}$ model from Feigenbaum and Dafalias (2008). However, it must be pointed out that if one would like to simulate also the distortion of the yield surface shape, then the $\mathcal{A}$ model is definitively superior to the $\boldsymbol{\alpha}$ and $\mathbf{r}$ models as shown in Feigenbaum and Dafalias (2007, 2008). Comparing the various kinematic hardening rules (with or without distortion), it seems that, of those studied MAFTr generally performs the best, although MAFMr performs nearly as well, and generally the variable r as the weight factor performs better than the fixed $\delta = 0.5$ with the BCD modification.

Now that it has been shown that directional distortional hardening can dramatically improve predictions of biaxial stress controlled ratcheting, in order to make use of these models in real engineering applications of ratcheting problems it is imperative that a systematic calibration technique be developed. Current work is underway to develop such a technique.

Acknowledgments

The authors would like to acknowledge the National Science Foundation Grant No. 1012066 for their financial support and fostering this collaboration. H.P. Feigenbaum and J. Dugdale would like to acknowledge funding from NAU's Faculty Grants Program. Y.F. Dafalias would like to acknowledge funding from the European Research Council under the European Union's Seventh Framework Program(FP7/2007-2013)/ERC IDEAS Grant Agreement No. 290963 (SOMEF).

References

Armstrong, P.J., Frederick, C.O., 1966. A mathematical representation of the multiaxial baushinger effect. Tech. Rep. RD/B/N 731, General Electric General Board.

Bari, S., Hassan, T., 2000. Anatomy of coupled consititutive models for ratcheting simulation. International Journal of Plasticity 16, 381–409.
Bari, S., Hassan, T., 2002. An advancement in cyclic plasticity modeling for multiaxial ratcheting simulation. International Journal of Plasticity 18, 873–894.
Boucher, M., Cayla, P., Cordebois, J.P., 1995. Experimental studies of yield surfaces of aluminum alloy and low carbon steel under complex biaxial loadings. European Journal of Mechanics, A/Solids 14 (1), 1–17.
Burlet, H., Cailletaud, G., 1986. Numerical techniques for cyclic plasticity at variable temperature. Engineering Computations 3 (2), 143–153.
Chaboche, J.L., 1991. On some modifications of kinematic hardening to improve the description of ratcheting effects. International Journal of Plasticity 7, 661–678.
Chaboche, J.L., Dang-Wan, K., Cordier, G., 1979. Modelization of the strain memory effect on the cyclic hardening of 316 stainless steel. In: SMIRT-5, Divsion L, Berlin.
Corona, E., Hassan, T., Kyriakides, S., 1996. On the performance of kinematic hardening rules in predicting a class of biaxial ratcheting histories. International Journal of Plasticity 12 (1), 117–145.
Dafalias, Y.F., 1979. Anisotropic hardening of initially orthotropic materials. ZAMM 59, 437–446.
Dafalias, Y.F., Feigenbaum, H.P., 2011. Biaxial ratcheting with novel variations of kinematic hardening. International Journal of Plasticity 27 (4), 479–491.
Dafalias, Y.F., Kourousis, K.I., Saridis, G.J., 2008a. Multiplicative AF kinematic hardening in plasticity. International Journal of Solids and Structures 45, 2861–2880.
Dafalias, Y.F., Kourousis, K.I., Saridis, G.J., 2008b. Corrigendum to multiplicative AF kinematic hardening in plasticity. International Journal of Solids and Structures 45, 4878.
Dafalias, Y.F., Schick, D., Tsakmakis, C., 2002. A simple model for describing yield surface evolution. In: Hutter, K., Baaser, H. (Eds.), Lecture Note in Applied and Computational Mechanics. Springer Verlag, Berlin, pp. 169–201.
Delobelle, P., Robinet, P., Boucher, L., 1995. Experimental study and phenomenological modelization of ratchet under uniaxial and biaxial loading on an austenitic stainless steel. International Journal of Plasticity 11 (4), 295–330.
Feigenbaum, H.P., Dafalias, Y.F., 2007. Directional distortional hardening in metal plasticity within thermodynamics. International Journal of Solids and Structures 44, 7526–7542.
Feigenbaum, H.P., Dafalias, Y.F., 2008. Simple model for directional distortional hardening in metal plasticity within thermodynamics. ASCE Journal of Engineering Mechanics 134 (9), 730–738.
François, M., 2001. A plasticity model with yield surface distortion for non proportional loading. International Journal of Plasticity 17, 703–717.
Guionnet, C., 1992. Modeling of ratcheting in biaxial experiments. ASME Journal of Engineering Materials and Technology 114, 56–62.
Hassan, T., Corona, E., Kyriakides, S., 1992. Ratcheting in cyclic plasticity, Part II: Multiaxial behavior. International Journal of Plasticity 8, 117–146.
Hassan, T., Kyriakides, S., 1992. Ratcheting in cyclic plasticity, Part I: Uniaxial behavior. International Journal of Plasticity 8, 91–116.
Kurtyka, T., Zyczkowski, M., 1996. Evolution equations for distortional plastic hardening. International Journal of Plasticity 12 (2), 191–203.
McComb, H.G., June 1960. Some experiments concerning subsequent yield surfaces in plasticity. Tech. Rep. D-396, National Aeronautics and Space Adminstration.
Naghdi, P.M., Essenburg, F., Koff, W., 1958. An experimental study of initial and subsequent yield surfaces in plasticity. Journal of Applied Mechanics 25 (2), 201–209.
Ohno, N., Wang, J.D., 1993. Kinematic hardening rules with critical state of dynamic recovery, Part I: formulations and basic features for ratcheting behaviour. International Journal of Plasticity 9, 375–390.
Phillips, A., Tang, J.-L., Ricciuti, M., 1975. Some new observations on yield surfaces. Acta Mechanica 20, 23–39.
Plesek, J., Feigenbaum, H.P., Dafalias, Y.F., 2010. Convexity of yield surfaces with directional distortional hardening. ASCE Journal of Engineering Mechanics 136 (4), 477–484.
Prager, W., 1935. Der Einglu der Verformung af die Fliebedingung zähplastischer Körper. ZAMM 15 (1/2), 76–80.
Prager, W., 1956. A new method of analyzing stresses and strains on work-hardening plastic solids. ASME Journal of Applied Mechanics 23, 493–496.
Shutov, A.V., Panhans, S., Krieig, R., 2011. A phenomenological model of finite strain viscoplasticity with distortional hardening. ZAMM – Journal of Applied Mathematics and Mechanics 91 (8), 653–680.
Voyiadjis, G.Z., Foroozesh, M., 1990. Anisotropic distortional yield model. Journal of Applied Mechanics 57, 537–547.
Wu, H.C., Yeh, W.C., 1991. On the experimental determination of yield surfaces and some results of annealed 304 stainless steel. International Journal of Plasticity 7, 803–826.